Florida State University Libraries

2018-03-13

Mechanistic Origins Of Enzyme Activation In Human Glucokinase Variants Associated With Congenital Hyperinsulinism

Shawn M. Sternisha, Peilu Liu, Alan G. Marshall and Brian G. Miller

The publisher's version of record is available at https://doi.org/10.1021/acs.biochem.8b00022

Follow this and additional works at DigiNole: FSU's Digital Repository. For more information, please contact lib-support@fsu.edu

Mechanistic Origins of Enzyme Activation in Human Glucokinase Variants Associated with Congenital Hyperinsulinism

Shawn M. Sternisha[1], Peilu Liu[1], Alan G. Marshall[1,2] and Brian G. Miller[1*]

[1]Department of Chemistry and Biochemistry, Florida State University, Tallahassee, Florida 32306, USA

[2] Ion Cyclotron Resonance Program, The National High Magnetic Field Laboratory, Tallahassee, Florida 32310, USA

*Corresponding author:

4005 Chemical Sciences Lab, Department of Chemistry and Biochemistry, Florida State University, Tallahassee FL 32303; miller@chem.fsu.edu; 850-645-6570.

Submitted to *Biochemistry* (MS # bi-2018-00022v): **8 January, 2018**

Revised MS submitted: **8 February, 2018**

Abstract

Human glucokinase (GCK) acts as the body's primary glucose sensor and plays a critical role in glucose homeostatic maintenance. Gain-of-function mutations in *gck* produce hyperactive enzyme variants that cause congenital hyperinsulinism. Prior biochemical and biophysical studies suggest that activated disease variants can be segregated into two mechanistically distinct classes, termed α-type and β-type. Steady-state viscosity variation studies indicate that the k_{cat} values of wild-type GCK and an α-type variant are partially diffusion-limited, whereas the k_{cat} value of a β-type variant is viscosity-independent. Transient-state chemical quench-flow analyses demonstrate that wild-type GCK and the α-type variant display burst kinetics, whereas the β-type variant lacks a burst phase. Comparative hydrogen-deuterium exchange mass spectrometry of unliganded enzymes demonstrates that a disordered active-site loop, which folds upon glucose binding, is protected from exchange in the α-type variant. The α-type variant also displays increased exchange within a β-strand located near the enzyme's hinge region, which becomes more solvent-exposed upon glucose binding. In contrast, β-type activation causes no substantial difference in global or local exchange relative to unliganded, wild-type GCK. Together these results demonstrate that α-type activation results from a shift in the conformational ensemble of unliganded GCK toward a state resembling the glucose-bound conformation, whereas β-type activation is attributable to an accelerated rate of product release. This work elucidates the molecular basis of naturally occurring, activated GCK disease variants and provides insight into the structural and dynamic origins of GCK's unique kinetic cooperativity.

Introduction

Glucokinase (GCK) is one of four human hexokinase isozymes that catalyze the ATP-dependent phosphorylation of glucose. GCK is expressed in pancreatic β-cells, where it governs glucose-stimulated insulin secretion, and in hepatoparenchymal cells, where it participates in glycogen synthesis.[1,2] GCK exhibits unique kinetic attributes that are responsible for its role in glucose homeostasis.[3] The enzyme displays a midpoint glucose responsiveness value ($K_{0.5}$ = 8 mM) that correlates with physiological glucose concentrations in the blood stream.[4,5] GCK also displays mild cooperativity toward glucose, which is characterized by a Hill coefficient of 1.7, resulting in a sigmoidal kinetic response to glucose. Inactivating or loss-of-function genetic lesions in the *gck* gene result in maturity onset diabetes of the young (MODY) and permanent neonatal diabetes mellitus (PNDM).[6–8] In contrast, mutations producing hyperactive GCK variants lead to persistent hyperinsulinemic hypoglycemia of infancy (PHHI, also known as congenital hyperinsulinism), the severity of which scales with the level of GCK activation.[6]

Cooperativity in GCK is of particular interest because GCK functions as a monomer and contains only one binding site for glucose. Thus, the origin of the allosteric features of this enzyme is distinct from that of typical cooperative enzymes.[5,9,10] Previous nuclear magnetic resonance (NMR) studies in our lab demonstrated that GCK's kinetic cooperativity is governed by slow, millisecond timescale structural transitions within the enzyme's small domain.[11,12] These conformational transitions occur with a rate constant, k_{ex}, comparable to the enzyme's catalytic rate constant, k_{cat}, and the temporal equivalence between these two processes is required for the generation of a sigmoidal steady-state response.[13–15] Based on the totality of biochemical and biophysical data collected to date, the loss of cooperativity that accompanies PHHI-associated activation is expected to occur when the values of either k_{ex} or k_{cat} are altered such that they are no longer of comparable magnitude. Understanding the detailed mechanistic origins of

activated GCK variants promises to provide insight into the structural, functional, and dynamic basis of the enzyme's unique form of monomeric allostery.[16,17]

Using a combination of genetic selection, limited proteolysis, and NMR studies, we recently reported two functionally distinct mechanisms of GCK activation that are operational in both clinically discovered and genetically engineered enzyme variants.[13] In the first activation scheme, coined α-type activation, proteolytic susceptibility of a mobile active site loop is diminished, the enzyme's affinity for glucose is increased, and the 2D ^{1}H-^{13}C heteronuclear multiple quantum coherence (HMQC) ^{13}C-Ile NMR spectrum of the unliganded enzyme appears qualitatively similar to that of the glucose-bound, wild-type enzyme. The α-type activation mechanism appears to be the mode of action for small molecule allosteric activators that have been explored as potential therapeutic agents for MODY.[18] In β-type activation, however, the proteolytic susceptibility of the active site loop is enhanced, suggestive of alterations in the structure and/or dynamics of the loop, while the glucose affinity and the ^{13}C-Ile NMR spectrum appear unchanged from the wild-type enzyme.[13] These observations are suggestive of a model in which α-type activation perturbs the thermodynamic distribution of enzyme conformations in favor of a state preorganized for glucose binding, whereas β-type activation operates by a different, less structurally perturbative mechanism. The goal of the present study is to test this postulated model for α-type and β-type activation and to provide a more detailed description of the structural and functional alterations present in each variant.

Prior NMR experiments were limited in describing the structural differences between wild-type GCK and each activated variant, since they relied on only 17 sparsely distributed isotopic labels located on isoleucine side chain.[13] To provide a more complete picture of the structural consequences of enzyme activation, here we report the results of comparative

hydrogen-deuterium exchange mass spectrometry (HDX-MS) of wild-type GCK and representative activated variants. Unlike our previous NMR experiments[11-13], these experiments probe alterations to the polypeptide backbone, providing coverage across more than 90% of the primary sequence. We combine these structural investigations with viscosity variation studies and chemical quench-flow kinetic analyses to investigate mechanistic differences associated with steps that contribute to the k_{cat} value for each enzyme. Together, our results provide a detailed description of the molecular origins and functional alterations that occur in activated, disease-associated variants.

Materials and Methods

Protein expression and purification

Human pancreatic glucokinase was expressed as an N-terminal hexa-histidine tagged polypeptide from pET-22b(+) in BL21(DE3) *E. coli* cells. Cultures were inoculated to an initial $OD_{600\ nm}$ of 0.01 in Luria-Bertani (LB) broth supplemented with ampicillin (100 µg/mL). Cells were grown at 37 °C and 250 rpm until the $OD_{600\ nm}$ reached 0.7, at which point the temperature was reduced to 20 °C. Once the incubator reached 20 °C, IPTG (1 mM) was added to induce gene expression and growth was continued for 20 h. The α-13 helix variant[19] was produced in an identical manner. For the β-hairpin variant[13], an LB-agar plate was streaked from a frozen stock of BL21(DE3) cells harboring the expression vector. An isolated colony from the plate was used to inoculate LB broth supplemented with ampicillin (100 µg/mL) and cells were grown at 37 °C and 250 rpm. Once the OD_{600} reached 0.7, sufficient culture was harvested by centrifugation at 8,000 x *g* for 10 min to inoculate complete M9 minimal medium to an initial $OD_{600\ nm}$ of 0.15. Complete M9 medium contained M9 salts [(Na_2HPO_4 (30 g/L), KH_2PO_4 (15 g/L), NaCl (2.5 g/ L), pH 8.0], ampicillin (100 µg/mL), NH_4Cl (1 g/L), thiamine (25 µg/mL),

$FeSO_4$ (10 µM), $MgSO_4$ (1 mM), Metal Mix [$FeCl_3$ (16.2 mg/L), $ZnCl_2$ (1.44 mg/L), $CoCl_2$ (1.2 mg/ L), Na_2MoO_4 (1.2 mg/L), $CaCl_2$ (0.6 g/L), $CuSO_4$ (190 mg/ L), H_2CO_3 (5 mg/L), and 0.37 mL of HCl], and 1.3% v/v glycerol as the sole carbon source. Once the OD_{600} reached 0.7, the temperature was reduced to 20 °C, IPTG (1 mM) was added to induce gene expression, and growth was continued for 36 hours.

Cells were harvested via centrifugation at 8,000 x *g* and 4 °C for 10 min. The resulting cell pellets were resuspended in cold buffer A (5 mL/g of pellet) containing potassium phosphate (50 mM, pH 7.6), KCl (50 mM), dithiothreitol (10 mM), imidazole (25 mM), and glycerol (25% v/v), and cells were lysed via French press. Crude cell lysates were centrifuged at 25,000 x *g* and 4 °C for 30 min and the cleared cell lysates were loaded onto a 5 mL HisTrap FF affinity column equilibrated in cold buffer A. The column was washed with 10 column volumes of cold buffer A and GCK was eluted with cold buffer B (buffer A supplemented with 250 mM imidazole). GCK was dialyzed at 4 °C against 1 L of size exclusion chromatography (SEC) buffer containing potassium phosphate (50 mM, pH 7.6), KCl (50 mM), and dithiothreitol (10 mM). Following dialysis, GCK was concentrated to ~300 µM by use of an Amicon Ultra-15 Centrifugal Filter Unit (EMD Millipore) and injected onto a Superdex 200 column (GE Healthcare) pre-equilibrated in SEC buffer. The gel filtration column was run at a flow rate of 0.2 mL/min, and fractions containing the highest $A_{280\ nm}$ values were pooled and retained for analysis. Protein concentrations were determined spectrophotometrically based on calculated molecular weights and an extinction coefficient (ε) of 32,890 M^{-1} cm^{-1}. Chemicals were purchased from Fisher Scientific and Sigma-Aldrich.

Viscogen variation studies

GCK activity was assayed spectrophotometrically at 340 nm by coupling the production of glucose 6-phosphate to the reduction of NADP+ via glucose 6-phosphate dehydrogenase (G6PDH) at 25 °C by use of a Cary 100 UV-Vis spectrophotometer. Reaction mixtures contained HEPES (0.25 M, pH 7.6), NADP+ (0.5 mM), KCl (50 mM), DTT (10 mM), ATP (10 mM), glucose (0.2 M), $MgCl_2$ (12 mM), and G6PDH (7.5 units). Assays were run in triplicate and initiated by addition of ATP. The slope of the linear portion of the progress curves yielded steady-state velocities. The dependence of k_{cat} upon solution microviscosity was assessed with the above conditions with the inclusion of varied concentrations of sucrose or trehalose (0-30% w/v). Relative viscosities of sucrose and trehalose solutions were measured in triplicate by use of a Cannon-Fenske viscometer maintained at 25 °C in a circulating water bath according to the manufacturer's instructions. Relative maximal velocities were plotted against the corresponding relative viscosities and slopes for each plot were calculated by the linear least-squares method. Assays conducted at pH 5.5 required 15 units of G6PDH, an amount empirically determined by conducting assays with increasing amounts of G6PDH until the coupling enzyme was not limiting the reaction velocity.

Chemical quench-flow kinetic assays

Pre-steady-state experiments were carried out in triplicate with a calibrated KinTek RQF-3 Rapid Quench-Flow Instrument maintained at 25 °C by a circulating water bath. One sample syringe was loaded with a solution containing GCK (55-410 μM), HEPES (50 mM, pH 7.6), KCl (50 mM), DTT (10 mM), glucose (0.2 M), while the other sample syringe was loaded with a solution containing HEPES (50 mM, pH 7.6), KCl (50 mM), DTT (10 mM), ATP (50 mM), $MgCl_2$ (60 mM), and glucose (0.2 M). Reactions were initiated by the rapid mixing of aliquots (~18 μL) of reactants from both syringes, and reactions were quenched at time intervals ranging

from 10-500 ms based on a final concentration of 1M EDTA (pH 8.3). The individual reaction mixtures were collected in pre-weighed 1.5 mL microtubes and immediately frozen in a dry ice-ethanol slurry. The reaction mixtures were then thawed, mixed with an additional 50 µL of EDTA (1 M, pH 8.3), supplemented with 5 µL NADP+ (100 mM), and diluted to 495 µL with HEPES (50 mM, pH 7.6), KCl (50 mM), DTT (10 mM). By use of a Cary 100 UV-Vis spectrophotometer, the net change in absorbance upon the addition of 5 µL (2.5 units) of G6PDH was measured to determine the amount of G6P produced by GCK at each time interval.

Hydrogen-deuterium exchange mass spectrometry

Hydrogen/deuterium exchange (HDX) was performed as previously described by use of an automated HTC Pal auto-sampler (Eksigent Technologies, Dublin, CA).[20] To initiate each hydrogen-deuterium exchange period, 5 µL of purified GCK was mixed with 45 µL of corresponding D_2O buffer (50 mM KPO_4, 50 mM KCl, 10 mM DTT, pH 7.6). For the blank control, the dilution was performed in H_2O buffer. Triplicate reactions were conducted at 1-2 °C, to reduce back-exchange, for reaction periods of 0.5, 1, 4, 15, 30, 60, and 480 min. Each sample was quenched by rapid mixing with 25 µL of 200 mM tris(2-carboxyethyl)phosphine, and 8 M urea in 1.0% formic acid, followed by proteolysis for 3 min by addition of 25 µL of a 40% saturated protease type XIII solution in 1.0% formic acid (final pH meter reading ~2.3). After proteolysis, the resulting peptides were separated and desalted on a Pro-Zap MS C_{18} column (1.5 µm, 2.1 x 10 mm; Dr. Maisch Gmbh, Ammerbuch, Germany) by use of a Jasco HPLC. A rapid gradient from 2% to 95% B over 2 min (A, acetonitrile/H_2O/formic acid, 5/94.5/0.5; B, acetonitrile/H_2O/formic acid, 95/4.5/0.5) was performed to elute peptides at a flow rate of 0.3 mL/min. The eluted peptides were directed into a positive electrospray ionization 21 tesla Fourier transform ion cyclotron resonance mass spectrometer (FT-ICR MS) for measurement.

Mass spectra were collected from *m/z* 400 ~ 1300 at a high resolving power ($m/\Delta m_{50\%}$ = 300,000 at *m/z* 400). Identities of peptides were determined by accurate mass alone without any fragmentation techniques. Data were analyzed with a previously described custom software package.[21,22] The average relative deuterium uptake difference (ARDD) between each pair of GCK samples was calculated from the following equation:

$$\text{ARDD} = \sum_i \frac{A(t_i) - B(t_i)}{A(t_i)} \quad (1)$$

in which *A* is the deuterium uptake for sample (activated GCK variant) after a stated reaction period (t_i) and *B* (wild-type GCK) is deuterium uptake for sample *B* after the same reaction period (t_i).[23]

Results and Discussion

To investigate the extent to which the k_{cat} value of wild-type GCK reports on a diffusion-limited process, such as product release, we performed enzyme assays under saturating substrate concentrations in the presence of the microviscogen sucrose.[24] A plot of the relative k_{cat} value ($k_{cat}°/k_{cat}$) as a function of relative solution viscosity (η_{rel}), revealed a slope of 0.31, suggesting that the k_{cat} value is partially diffusion-limited (Figure 1A). To ensure that the observed viscosity dependence was independent of viscogen identity, we performed identical experiments in the presence of increasing concentrations of trehalose. With trehalose as a microviscogen, the slope was 0.37, in agreement with experiments involving sucrose (Figure 1A). We also performed viscosity variation studies at pH 5.5, at which the chemical transformation step is expected to be rate-limiting. Under these conditions, the solution microviscosity did not influence the enzyme's k_{cat} value, demonstrating that that the experiments were indeed reporting on diffusion limited processes (Figure 1A). Collectively, these data support the conclusion that the k_{cat} value of wild-

Figure 1. Relative k_{cat} values of (A) Wild-type GCK, (B) α-13 Helix GCK, and (C) β-hairpin GCK as a function of relative solution microviscosity. Error bars are ± standard deviation (n = 3).

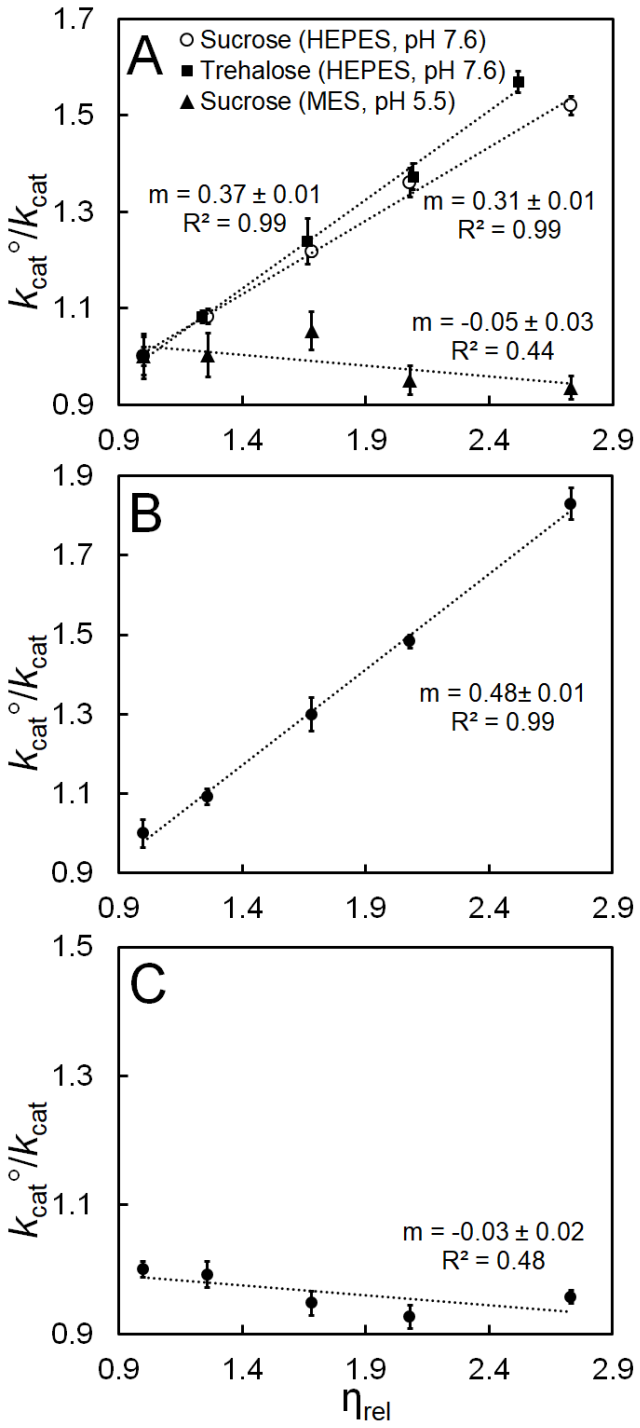

type human GCK is partially limited by the rate of product release. Our results do not exclude the possibility that a conformational change after product release contributes to the rate-limiting step, although such reorganization(s) are not expected to display a linear dependence upon relative viscosity.[25]

We also conducted viscosity variation studies for previously described α-13 helix and β-hairpin variants of GCK, which serve as prototypic representatives of the α-type and β-type activation mechanisms.[13,19] A plot of the relative k_{cat} value as a function of relative solution viscosity for the α-variant revealed a slope of 0.48, demonstrating that the k_{cat} value is partially limited by the rate of product release for this activated enzyme (Figure 1B). Conversely, viscosity variation studies with the β-type variant revealed a slope of -0.03 (Figure 1C), indicating that product release no longer contributes to the k_{cat} value for this enzyme. The substitutions present within the β-hairpin variant are localized to a mobile active site loop that undergoes a disorder-order transition upon glucose binding.[13] Based on our viscosity variation studies, we postulate that the activating substitutions in β-type GCK alter the structure and/or dynamics of the loop such that product release is accelerated. Analysis of available GCK crystal structures reveals that a hydrogen-bonding network at the base of the loop is disrupted by the substitutions present in the β-hairpin variant, which could facilitate rapid product release (Figure S1). In contrast, our viscosity variation studies indicate that α-type activation is not accompanied by an accelerated rate of product release.

Chemical quench-flow analysis is a well-established method to test for the existence of a pre-steady-state burst in product formation and to quantify individual microscopic rate constants that contribute to the value of k_{cat}.[26–28] Our viscosity variation results suggest that wild-type GCK, as well as the activated α-variant, might display burst phase kinetics attributable to the

existence of one or more steps preceding partially rate-limiting product release. To investigate this possibility, and to uncover quantitative information about microscopic steps that remain cloaked in steady-state kinetic analyses, we performed chemical quench-flow experiments on wild-type GCK and both α- and β-type activated variants.[29-31] Reproducible chemical quench-flow data were obtained for all three enzymes across a time window spanning 20-500 msec. Visual inspection of the quench-flow data for wild-type GCK and the α-13 helix variant was suggestive of a biphasic profile, whereas the β-hairpin data appeared monophasic (Figure 2).

In an attempt to quantify individual rate constants for each phase, we globally fitted our data to a three-step, bisubstrate reaction model by use of KinTek Explorer software (Figure S2).[32,33] During fitting, the ratio of rate constants for ATP binding and release (k_{off}/k_{on}) was constrained at 0.5 mM to reflect the experimentally determined ATP K_m value. We also constrained the chemical (k_2) and product release (k_3) steps to be irreversible. Based on this model, global fit analyses yielded rate constants for the product release step that closely matched the k_{cat} values determined from steady-state assays for wild-type GCK and for both activated variants (Table S1). However, poor estimates were obtained for the chemical step. The expected upper limit for the half-life for the burst phase is ~25 msec, as calculated based upon the recognition that it should be faster than the steady-state k_{cat} value. This value approaches the lower limit accessible by the quench flow instrument used in this study, as quench flow data collected below 20 milliseconds was associated with large quantification errors. We attribute the inability to obtain reasonable estimates for the rate constant of the chemical step to a lack of sufficient quench-flow kinetic data at short time intervals.

Despite the inability to quantify the burst phase via global fit analysis, several lines of evidence support the existence of one or more steps preceding product release for wild-type

Figure 2. Linear regression analysis of representative quench-flow data for (A) 120 μM wild-type GCK, (B) 88 μM α-13 helix GCK, and (C) 55 μM β-hairpin GCK. Solid data points represent the steady-state phase and open data points represent a fast linear phase spanning the first 100 msec. Dashed lines represent extrapolation of the steady-state phase to a nonzero y-intercept. Error bars are ± standard deviation (n = 3).

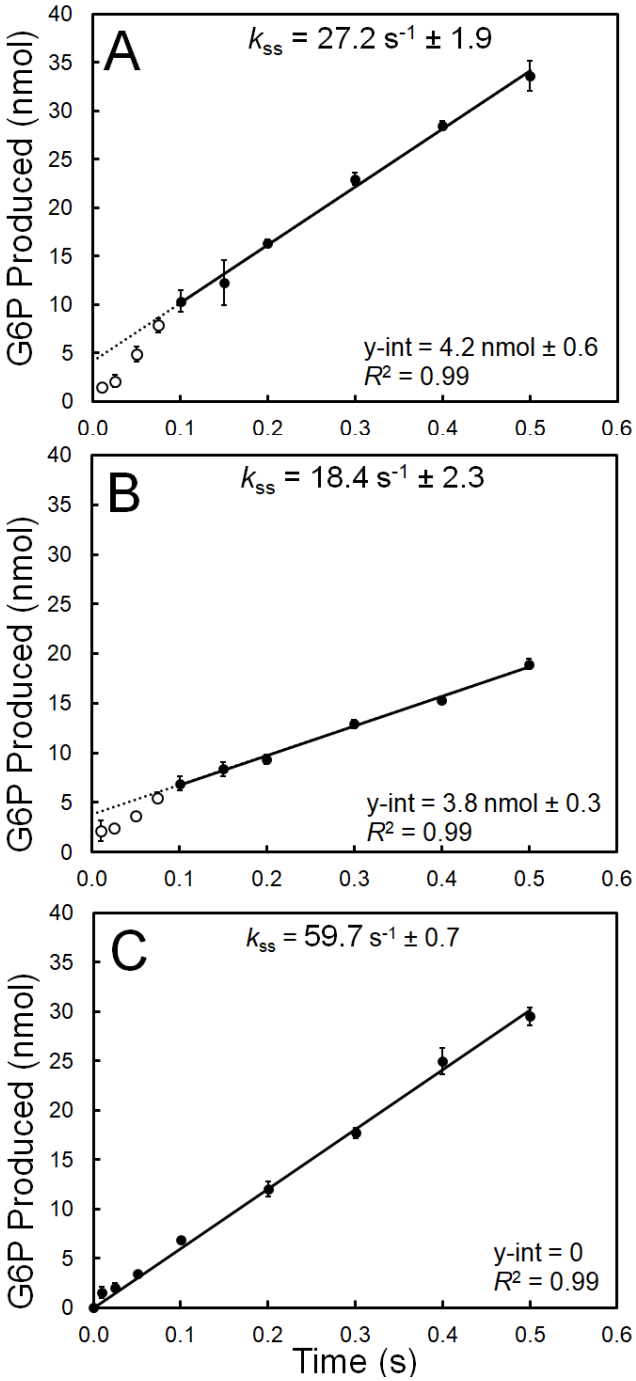

GCK and the α-variant. Linear extrapolation of the quench-flow data from the steady-state regime, considered here to be represented by data at 100 milliseconds and above, yielded non-zero y-intercept values for both enzymes (Figure 2A, B). Using 120 μM wild-type GCK, we observed a y-intercept of 4.2 nmol (233 μM) of glucose 6-phosphate (G6P), and for experiments involving the α-13 helix variant at a concentration of 88 μM, the y-intercept was 3.8 nmol (211 μM) of G6P. The observation that the y-intercepts do not traverse the origin is consistent with the existence of one or more steps preceding the partially rate-limiting product release for both enzymes. In contrast, the y-intercept of the steady-state rate displayed by 55 μM β-hairpin GCK was significantly closer to the origin. Constraining the y-intercept of the β-activated variant to zero provides a good linear fit (R^2 = 0.99), suggesting that a pre-steady-state burst phase is unnecessary to explain the quench-flow data for this enzyme.

When a pre-steady-state burst is present, the amplitude of the burst phase should correlate with the concentration of the enzyme used in the experiment. Indeed, we observed a correlation between enzyme concentration and the y-intercept obtained from linear extrapolation of quench flow data from the steady-state regime when we performed quench flow experiments at variable concentrations of wild-type GCK. As enzyme concentration was increased, the value of the y-intercept obtained from linear extrapolation of quench flow data from the steady-state regime also increased. In cases for which the rate constants of the burst and steady-state phases do not differ significantly, the amplitude of the burst does not provide an accurate measure of the enzyme concentration.[30,34,35] The partial viscosity dependence observed for wild-type GCK and the α-variant suggested that this condition is likely true for both enzymes. This situation offers an explanation for the apparent discrepancy between the extrapolated y-intercept values and the enzyme concentrations shown in Figures 2A and 2B. Taken together, the quench-flow results

support a model in which the k_{cat} values of wild-type GCK and the α-type variant include contributions from one or more steps preceding the partially rate-limiting product release step. In contrast, the k_{cat} value for β-type variant reports on a different physicochemical process, which is not associated with product release.

Solution-phase amide hydrogen-deuterium exchange mass spectrometry (HDX-MS) provides a sensitive valuable complement to X-ray crystallography and NMR to probe protein structure and dynamics. HDX-MS is particularly useful for comparing differences in solvent-accessible surface areas within a series of related protein variants.[36–39] To gauge the applicability of HDX-MS in probing structural differences between wild-type and activated GCK variants, we first explored the enzyme's proteolytic susceptibility under acidic conditions. Without any exposure to D_2O, wild-type and activated GCK variants were denatured, digested by protease XIII, and subjected to LC-MS analysis. We found that treatment with protease XIII yielded 106 common peptides that spanned 93% of the primary sequence of GCK (Figure S3) with many overlapping segments to provide peptide-level sequence resolution. Here, high sequence coverage and a high number of overlapping peptides ensured a reliable conformational comparison. Using this protease and a previously developed automated HDX-MS method[20], we measured the average relative deuterium uptake differences (ARDD) between each activated variant and wild-type GCK. We found that segments 53-73, 159-186, and 275-302 of the α-13 helix variant display apparent alterations in deuterium exchange relative to wild-type GCK (Figure 3). Conversely, HDX-MS experiments failed to reveal significant (greater than 10%) ARDD differences between β-hairpin GCK and wild-type GCK in any region of the protein (Figure S4). These results indicate that α-type activation, but not β-type activation, is associated with changes in the structure and/or dynamics of specific regions of the unliganded enzyme.

To gain mechanistic insight into the differences in H/D exchange observed in the α-activated variant, we mapped ARDD values for each region onto the homolog crystal structures of both unliganded and glucose bound GCK. As shown in Figure 4, regions that exhibited reduced deuterium uptake in the α-variant include a mobile active site loop comprised of residues 159-180 and a peptide segment spanning residues 275-302. The observation of significantly decreased deuteration level in segment 159-180 is attributed to a disorder/order transition upon glucose binding, in accord with previous NMR data.[13] Segment 275-302 comprises part of the glucose-binding pocket; therefore, its decrease in deuteration level likely results from the formation of a more closed conformation, which limits the proton exchange with surrounding deuterium solvent (Figure 4, top). Conversely, we observed that a segment of the α-variant spanning residues 64-73 exhibited elevated levels of deuterium incorporation compared to its wild-type counterpart (labeled in red in Figure 3). This region is located within a loop/β-strand motif that connects the large and small domains.[40] Notably, previous studies have identified several activating substitutions within this region, including S64P, a variant that displays NMR features characteristic of the α-type activation mechanism.[11,17] HDX-MS revealed increased deuterium uptake in this region, in agreement with a comparison of the unliganded and glucose bound crystal structures, demonstrating that this region is more solvent-exposed in the glucose-bound state (Figure 4, bottom). HDX characterized data for activated GCK variants, in combination with prior NMR results,[11,13] provide compelling evidence that the unliganded α-activated GCK variant resembles the glucose bound conformation in several regions.

Conclusion

The present findings confirm the existence of two distinct mechanisms of activation for human GCK and establish the molecular basis for each activation process. Our combined

Figure 3. H/D exchange results for α-13 helix *versus* wild-type GCK, color-coded by deuteration level (%) onto the primary sequence of GCK. The relative deuterium uptake difference (ARDD, α-13 helix minus wild-type) is calculated from Equation 1. (Top) Primary sequence of GCK highlighting regions of differential deuterium uptake. Regions in which α-13 helix GCK exhibited increased deuterium exchange are shown in warm colors while regions in which α-13 helix GCK exhibited decreased deuterium exchange are shown in cool colors. The active site mobile loop is shown in the dashed red box. (Bottom) Deuterium uptake time-course results for wild-type and α-13 helix GCK for representative peptides 159-186, 53-61, 62-73, and 275-302. Deuterium uptake and maximum-entropy fits (smooth curves) vs $\log_{10}$ of H/D exchange reaction period. Blue: wild-type, Red: α-13 helix.

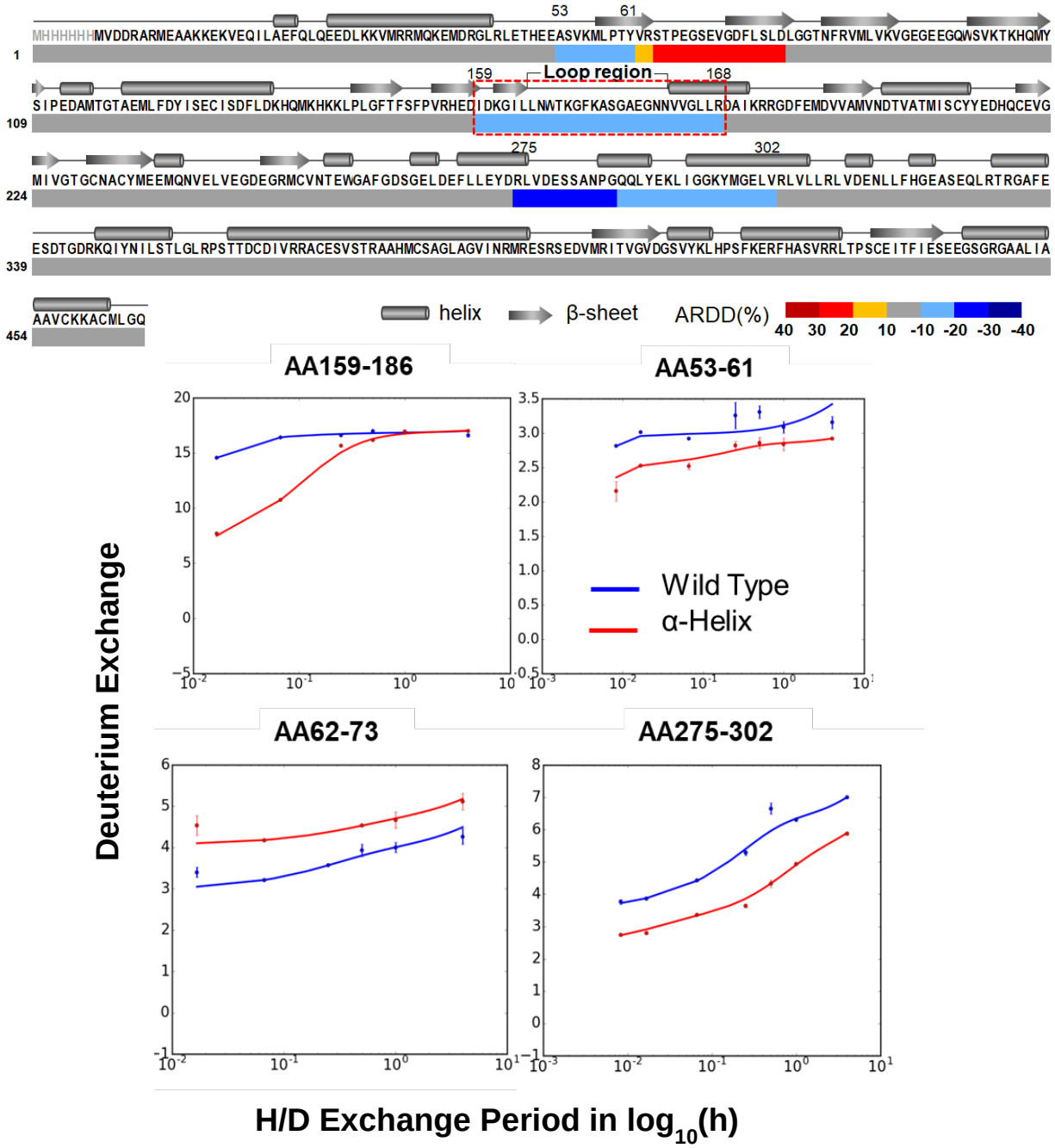

Figure 4: The average relative deuterium uptake differences (ARDD) for α-13 helix minus wild-type GCK mapped onto the crystal structures of wild-type GCK. (Top) Tertiary structure of glucose bound (left) and unliganded (right) GCK. (Bottom) ARDD mapped onto surface models of glucose bound (left) and unliganded (right) GCK. Regions in which α-13 helix GCK exhibited increased deuterium exchange are shown in warm colors while regions in which α-13 helix GCK exhibited decreased deuterium exchange are shown in cool colors. Protein Data Bank accession numbers for glucose bound and unliganded GCK are 1V4S and 1V4T.[41]

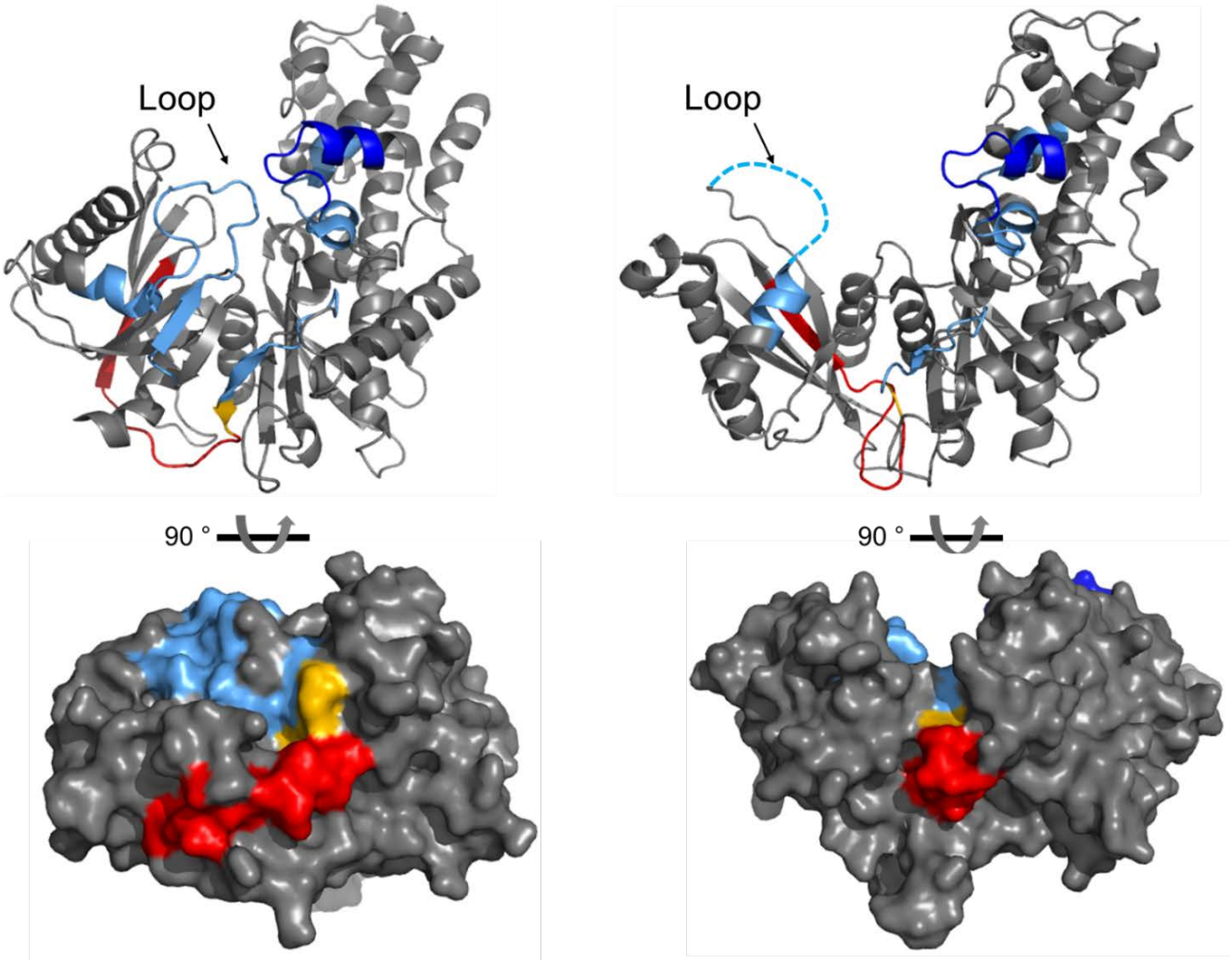

viscosity variation and chemical quench flow data indicate that β-type activation occurs via an acceleration of the product release step, such that it no longer partially limits the value of k_{cat}. HDX-MS analysis suggests that β-type activation is not accompanied by significant differences in enzyme backbone structure and/or dynamics. In contrast, α-type activation results from a shift in the conformational ensemble of unliganded GCK in favor of a state that resembles the glucose bound wild-type enzyme. This structural alteration does not appear to impact the partially rate-limiting process of product release or the presence of a burst phase, which is characteristic to both wild-type and α-type variants. Our HDX-MS results provide an improved level of understanding regarding the structural and dynamic origins of both activation mechanisms, as they substantially expand the data available from prior NMR investigations to include more than 90% of the polypeptide backbone for each enzyme.

Both types of activated variants investigated herein reduce the kinetic cooperativity of wild-type human GCK.[11-13] The observation that the Hill coefficient is reduced under these two mechanistically distinct activation schemes demonstrates the importance of both protein structure and dynamics for cooperativity. In particular, our results demonstrate that GCK can be activated by altering the enzyme's conformational ensemble or by mutations that perturb the kinetics of the partially rate-limiting product release step. Since both types of activated GCK variants can cause disease, our ability to uncover the underlying molecular origins of activation could facilitate the development of targeted therapeutic approaches to treat hyperinsulinemia unique to each type of activation mechanism.

Acknowledgements

The authors acknowledge P. Frantom for assistance in interpreting quench-flow results, K. Johnson for the generous gift of the Kintek Explorer software, and C. Mundoma of the Protein Biophysics Laboratory in the Institute for Molecular Biophysics at FSU for assistance with quench-flow experiments.

Author Contribution

S.M.S. and B.G.M. designed the research. S.M.S performed viscosity and quench-flow experiments and prepared the proteins. P.L. and A.G.M. designed the HDX-MS experiments, which were performed by P.L. S.M.S., B.G.M., P.L., and A.G.M analyzed the data. S.M.S., B.G.M., P.L., and A.G.M wrote the manuscript. All authors reviewed the results and approved the final version of the manuscript.

Funding

This work was supported, in part, by a grant from the National Institutes of Health (DK081358), NSF Division of Materials Research through DMR-11-57490, and the State of Florida.

Supporting Information

Figure S1: Disruption of the H-bonding network in the β-hairpin variant; Figure S2: Kintek Global Explorer analysis of the quench-flow data; Figure S3: Sequence coverage diagram for MS of tryptic digests; Figure S4: Deuterium uptake time course results for wild-type and β-hairpin GCK; Table S1: Rate constants derived from fitting quench-flow data by Kintek Global Explorer analysis.

Notes

The authors declare no competing financial interest.

References

1. Wilson, J. E. (1995) Hexokinases. *Rev Physiol Biochem Pharmacol*, 126, 65-198.
2. Ferre T., Riu E., Bosch F., and Valera A. (1996) Evidence from transgenic mice that glucokinase is rate limiting for glucose utilization in the liver. *FASEB J*, 10, 1213-1218.
3. Matschinsky, F. M. (1990) Glucokinase as glucose sensor and metabolic signal generator in pancreatic β-cells and hepatocytes. *Diabetes*, 39, 647-652.
4. Matschinsky, F. M. (2002) Regulation of pancreatic β-cell glucokinase: From basics to therapeutics. *Diabetes*, 51, S394-S404
5. Larion, M., and Miller, B. G. (2012) Homotropic allosteric regulation in monomeric mammalian glucokinase. *Arch Biochem Biophys*, 519, 103-111.
6. Osbak, K. K., Colclough, K., Saint-Martin, C., Colclough, Beer, N. L., Bellann-Chantelot, C., Ellard, S., and Gloyn, A. L. (2009) Update on mutations in glucokinase (GCK), which cause maturity-onset diabetes of the young, permanent neonatal diabetes, and hyperinsulinemic hypoglycemia. *Hum Mutat*, 230, 1512-1526.
7. Bell, G. I., and Polonsky, K. S. (2001) Diabetes mellitus and genetically programmed defects in beta-cell function. *Nature*, 414, 788-791.
8. Kim, S. H. (2015) Maturity-onset diabetes of the young: What do clinicians need to know? *Diabetes Metab J*, 39, 468-477.
9. Motlagh, H. N., Wrabl, J. O., Li, J., and Hilser, V. J. (2014) The ensemble nature of allostery. *Nature*, 508, 331-339.
10. Changeux, J-P. (2012) Allostery and the Monod-Wyman-Changeux model after 50 years. *Annu Rev Biophys*, 41, 103-133.
11. Larion, M., Salinas, R. K., Bruschweiler-Li, L., Miller, B. G., and Brüschweiler, R. (2012) Order-disorder transitions govern kinetic cooperativity and allostery of monomeric human glucokinase. *PLoS Biol*. 10, e1001452.
12. Larion, M., Hansen, A. L., Zhang, F., Bruschweiler-Li, L., Tugarinov, V., Miller, B. G., and Brüschweiler, R. (2015). Kinetic cooperativity in human pancreatic glucokinase originates from millisecond dynamics of the small domain. *Angew Chem Int Ed*, 54, 8129-8132.
13. Whittington, A. C., Ramsey, K. M., Larion, M., Brüschweiler, R., Bowler, J. M., and Miller, B.G. (2015) Dual allosteric activation mechanisms in monomeric human glucokinase. *Proc Natl Acad Sci U.S.A.*, 112, 11553-11558.

14. Lin, S. X., and Neet, K. E. (1990) Demonstration of a slow conformational change in liver glucokinase by fluorescence spectroscopy. *J Biol Chem*, 265, 9670-9675.

15. Frieden, C. (1970) Kinetic aspects of regulation of metabolic processes. The hysteretic enzyme concept. *J Biol Chem*, 245, 5788-5799.

16. Gloyn, A. L. (2003) Glucokinase (GCK) Mutations in hyper- and hypoglycemia: Maturity-onset diabetes of the young, permanent neonatal diabetes, and hyperinsulinemia of infancy. *Hum Mutat*, 22, 353-362.

17. Pal, P., and Miller, B. G. (2009) Activating mutations in the human glucokinase gene revealed by genetic selection. *Biochemistry*, 48, 814-816.

18. Bowler, J. M., Hervert, K. L., Kearley, M. L., and Miller, B. G. (2013) Small-molecule allosteric activation of human glucokinase in the absence of glucose. *ACS Med Chem Lett*, 4, 580-584.

19. Larion, M., and Miller, B. G. (2009) 23-Residue C-terminal α-helix governs kinetic cooperativity in monomeric human glucokinase. *Biochemistry*, 48, 6157-6165.

20. Frantom, P. A., Zhang, H. M., Emmett, M. R., Marshall, A. G., and Blanchard, J. S. (2009) Mapping of the allosteric network in the regulation of α-isopropylmalate synthase from Mycobacterium tuberculosis by the feedback inhibitor L-leucine: Solution-phase H/D exchange monitored by FT-ICR mass spectrometry. *Biochemistry*, 48, 7457-7464.

21. Kazazic, S., Zhang, H-M., Schaub, T.M., Emmett, M. R., Hendrickson, C. L., Blakney, G. T., and Marshall, A. G. (2010) Automated data reduction for hydrogen/deuterium exchange experiments, enabled by high-resolution Fourier transform ion cyclotron resonance mass spectrometry. *J Am Soc Mass Spectrom*, 21, 550-558.

22. Blakney, G. T., Hendrickson, C. L., and Marshall, A. G. (2011) Predator data station: A fast data acquisition system for advanced FT-ICR MS experiments. *Int J Mass Spectrom*, 306, 246-252.

23. Zhang, Q., Willison, L. N., Tripathi, P., Sathe, S. K., Roux, K. H., Emmett, M. R., Blakney, G. T., Zhang, H. M., and Marshall, A. G. (2011) Epitope mapping of a 95 kDa antigen in complex with antibody by solution-phase amide backbone hydrogen/deuterium exchange monitored by Fourier transform ion cyclotron resonance mass spectrometry. *Anal. Chem*. 83, 7129-7136.

24. Brouwer, A. C., and Kirsch, J. F. (1982) Investigation of diffusion-limited rates of chymotrypsin reactions by viscosity variation. *Biochemistry*, 21, 1302-1307.

25. Ansari, A., Jones, C. M., Henry, E. R., Hofrichter, J., and Eaton, W. A. (1992) The role of solvent viscosity in the dynamics of protein conformational changes, *Science* 256, 1796-1798.

26. Kellinger, M. W., and Johnson, K. A. (2011) Role of induced fit in limiting discrimination against AZT by HIV reverse transcriptase. *Biochemistry*, 50, 5008-5015.

27. Kellinger, M. W., and Johnson, K. A. (2010) Nucleotide-dependent conformational change governs specificity and analog discrimination by HIV reverse transcriptase. *Proc*

Natl Acad Sci U. S. A., 107, 7734-7739.

28. Bingaman, J. L., Messina, K. J., and Bevilacqua, P. C. (2017) Probing fast ribozyme reactions under biological conditions with rapid quench-flow kinetics. *Methods*, 120, 125-134.

29. Johnson, K. A. (1998) Advances in transient-state kinetics. *Curr Opin Biotechnol*, 9, 87-89.

30. Johnson, K. A. (1992) Transient-state kinetic analysis of enzyme reaction pathways. In: *The Enzymes: Mechanisms of Catalysis*, 20, 1-61

31. Fisher, H. F. (2005) Transient-state kinetic approach to mechanisms of enzymatic catalysis. *Acc Chem Res*, 38, 157-166.

32. Johnson, K. A., Simpson, Z. B., and Blom, T. (2009) Global Kinetic Explorer: A new computer program for dynamic simulation and fitting of kinetic data. *Anal Biochem*, 387, 20-29.

33. Johnson, K. A., Simpson, Z. B., and Blom, T. (2009) FitSpace Explorer: An algorithm to evaluate multidimensional parameter space in fitting kinetic data. *Anal Biochem*, 387, 30-41.

34. Copeland, R. A. (2000) *Enzymes: A Practical Introduction to Structure, Mechanism, and Data Analysis*. New York, NY. Wiley-VCH.

35. Johnson, K. A. (2013) A century of enzyme kinetic analysis, 1913 to 2013. *FEBS Lett*, 587, 2753-2766.

36. Thakur, A., Chandra, K., Dubey, A., D'Silva, P., Atreya, H. S. (2013) Rapid characterization of hydrogen exchange in proteins. *Angew Chemie - Int Ed*, 52, 2440-2443.

37. Busenlehner, L. S. and Armstrong, R. N. (2005) Insights into enzyme structure and dynamics elucidated by amide H/D exchange mass spectrometry. *Arch Biochem Biophys*, 433, 34-46.

38. Yan, X., and Maier, C. S. (2009) Hydrogen/deuterium exchange mass spectrometry. In: *Mass Spectrometry of Proteins and Peptides Methods in Molecular Biology*, 492, 255-271.

39. Pirrone, G. F., Iacob, R. E., and Engen, J. R. (2015) Applications of hydrogen/deuterium exchange MS from 2012 to 2014. *Anal Chem*, 87, 99-118.

40. Martinez, J. A., Larion, M., Conejo, M. S., Porter, C. M., and Miller, B. G. (2014) Role of connecting loop 1 in catalysis and allosteric regulation of human glucokinase. *Protein Sci*, 23, 915-922.

41. Kamata, K., Mitsuya, M., Nishimura, T., Eiki, J., and Nagata, Y. (2004) Structural basis for allosteric regulation of the monomeric allosteric enzyme human glucokinase. *Structure*, 12, 429-438.

TABLE OF CONTENTS GRAPHIC